frontiers in Earth Science

ORIGINAL RESEARCH
published: 01 March 2022
doi: 10.3389/feart.2022.843191

Mining-Induced Stress and Ground Pressure Behavior Characteristics in Mining a Thick Coal Seam With Hard Roofs

Zhijie Zhu[1,2]*, *Yunlong Wu*[1] and *Zhuang Liang*[3]

[1]School of Mining, Liaoning Technical University, Fuxin, China, [2]State Key Laboratory of Coal Mining and Clean Utilization, Beijing, China, [3]Research Centre, Ministry of Emergency Management, Beijing, China

The hard roof of coal mines has the characteristics of high hardness, good integrity, and large layer thickness, which leads to many ground control problems. To reveal the influence of a hard roof structure on the stress performance and coal pillar stability during mining operations, the 8,104 and 8,105 working faces in the Tongxin coal mine were considered as the research object to analyze the stress behavior during the working face advance. Numerical simulation software FLAC^{3D} was used to establish the numerical model of the longwall face under hard roof conditions. The stress distribution laws and coal pillar stability under different roof strengths were analyzed so as to explain the impacts of the hard roof on the stress distribution at the working face. The results show that during the second face proceeding, the influence zone of the front abutment pressure under hard roof conditions is 6 m wider than that under soft roof conditions, and the bearing stress at the working face is 10.4 MPa higher. At the mining position, the plastic zone of the pillar under hard roof conditions is 11 m wider than that under soft roof conditions, and the peak vertical stress is 5.13 MPa higher than that under soft roof conditions. At 25 m ahead of the working face, the plastic zone of the pillar under hard roof conditions is 6 m wider than that under soft roof conditions, and the peak vertical stress is 24.84 MPa higher than that under soft roof conditions. Additional overburden pressure produced by the uncaved hard roof increased pillar stress and plastic zones. Therefore, the hard roof is the main cause of strong ground pressure behavior in the Tongxin coal mine. Aiming at the strong mine pressure behavior, it is suggested to adopt the pre-splitting technology to reduce the influence of the hard roof on mine pressure.

Keywords: hard roof, longwall face, coal pillar stability, mining stress, pillar stress

OPEN ACCESS

Edited by:
Zhiqiang Yin,
Anhui University of Science and Technology, China

Reviewed by:
Hongchao Zhao,
Xinjiang University, China
Bangyou Jiang,
Shandong University of Science and Technology, China
Wu Cai,
China University of Mining and Technology, China

***Correspondence:**
Zhijie Zhu
zhuzhijie@lntu.edu.cn

Specialty section:
This article was submitted to Geohazards and Georisks, a section of the journal Frontiers in Earth Science

Received: *25 December 2021*
Accepted: *25 January 2022*
Published: *01 March 2022*

Citation:
Zhu Z, Wu Y and Liang Z (2022) Mining-Induced Stress and Ground Pressure Behavior Characteristics in Mining a Thick Coal Seam With Hard Roofs. Front. Earth Sci. 10:843191. doi: 10.3389/feart.2022.843191

1 INTRODUCTION

In coal mining, hard and difficult-to-collapse roofs refer to thick, stable, and hard rock layers such as sandstone, conglomerate, or limestone that occur above the coal seam or directly on the thin layer and have the characteristics of high strength, undeveloped joints and fissures, and large thickness. The hard roof structure is frequently encountered in many mining areas. In China, the quantity of coal seams with hard overlying strata accounts for about one third of the total reserves and are distributed in over than 50% of the mining districts (Yang et al., 2019). Datong coalfield is a most

typical area characterized by hard roof strata in China (Liu et al., 2021). During mining of the coal seam with hard roofs, it is difficult to effectively predict and overcome the accompanied problems such as roadway serious deformation, abnormal mine pressure, and engineering disasters. Existing theories of mine pressure and ground control cannot provide scientific guidance on dealing with these problems (Rajwa et al., 2020; Yang 2010; Zhang et al., 2021). Therefore, it is necessary to intensively study the instability mechanism when mining the coal seam with hard roofs and deeply understand the rules of ground pressure performance in hard-roof coal mining.

Wang et al., (2020) pointed out that the overlying strata will break and subside when mining the coal face in hard roof circumstances and believed the interaction among the broken rocks in the roof will produce a dynamic balance structure. Zonglong et al., (2006) presented the evolution model of hard roof breaking and elaborated the breaking mechanism of the hard roof. Mahini et al., (2013) developed a model of hard roof failure and learned the energy change during hard roof fracturing. Qin et al., (2019) calculated the collapse span of hard overlying rocks and explored the mechanism of hard roof caving. Taking the 8,939 working faces of the Xinzhouyao mine as the research site, Zhang et al., (2018) uncovered that when a hard roof breaks, a large amount of energy that is not beyond the critical value will be released by the broken rocks, leading to the coal and rock masses in an unstable state. Ardehjani et al., (2020) investigated the behavior of steep layers during the roof caving process in the gob space using numerical modeling. Bai and Tu (2016) used field observations and numerical simulation methods to investigate failure of a large span longwall drift under water-rich roofs. Das (2000) studied the splitting and caving characteristics of the strata's rocks and established the development of a roof–rock classification system to calculate the powered support capacity. Hosseini et al., (2014) calculated the periodic roof weighting interval in longwall mining using the finite element method. Ju et al., (2021) investigated the bedding adhesion strength on the stratified rock–roof fracture at the longwall coal mining face using physical and numerical methods. Juárez-Ferreras et al., (2008) proposed a new empirical formula to determine the roof pressure that the props must support, which fits longwall workings in Castile–Leon coalfields. Kang et al., (2018) created a large-scale physical model and a numerical model to study the roof failure mechanism, abutment pressure distribution, and collapsed roof pattern during longwall face retreat mining. Liu et al., (2017) studied the influence of the varying immediate roof thickness on the lower strong roof strata movement and failure pattern in longwall coal mining with a large mining height by field tests. Mohammadi et al., (2021) and Murmu and Budi (2021) presented a hybrid probabilistically qualitative–quantitative model to evaluate cavability of the immediate roof and to estimate the main caving span in longwall mining. Ning et al., (2017) investigated the mining-induced fracturing and the roof movement under the double-layer hard and thick roof *via* microseismic (MS) monitoring. Xu et al., (2015) investigated the fracturing and caving process of key strata in overburden strata and the distribution law of abutment stress over key strata and immediate roof and analyzed the effect of the rupture of key strata on abutment stress in the coal rib. Most researchers mainly focused on the structure of hard overburden, the length of roof caving, and the characteristics of overburden movement when studying the stress distribution and evolution in hard roof mines. Few efforts are made on the influence of hard roof strata on the stress behavior at the working face.

A total of 8,104 and 8,105 working faces in the Tongxin coal mine were selected as the study site in this work. The FLAC^{3D} numerical model is established to simulate the progression of the working face under different roof conditions. The influence of the stratified hard roof on the mining stress at the working face is analyzed. The influence of hard overlying rocks on the coal pillar stability was also surveyed by investigating the elastic–plastic zone and stress distribution in the coal pillar.

2 MINING CONDITIONS

The coal seam with a thickness of 15.3 m and a dip angle of 1–3° is buried at 448 m at Tongxin coal mine underground. The thickness changes a little on the whole. The roof is mainly sandstone with a steady occurrence. The roof is considered as a hard roof from the perspective of mechanical properties. The 8,104 working face is 207 m along the dip and 1932 m along the strike. A 45-m-wide pillar is reserved between the 8,104 and 8,105 working faces. The layout of the two working faces is shown in **Figure 1**. The working face adopts the comprehensive mechanized top coal caving mining methods. The mining height is 3.9 m, and the coal caving thickness is 11.59 m. Roof and floor strata distributions of three to five coal seams are shown in **Table 1**. There are three hard roofs above three to five coal seams. The section of the return air tunnel is a rectangular section, and the section size is width × height = 5,000 mm × 3,700 mm. The section of the transport roadway is a rectangular section, and the section size is width × height = 5,600 mm × 3,400 mm. The roadway adopts the joint support method of the anchor bolt, anchor cable, steel belt, and metal mesh. The spacing and row spacing of anchor bolts are 0.8 × 0.8 m, while cables are 1.6 × 1.6 m. The length of the anchor bolt and cable are 2.5 and 8.3 m.

The ground pressure behavior of fully mechanized caving face mining with the hard roof has the following characteristics:

1) The main roof first caving interval was about 130.8 m, and the periodic caving interval was about 18.3 m. Due to the large inclination length of the working face and the thickness of the top coal, the pressure of the working face was relatively large, which can reach more than 14,000 kN, and the pressure in the middle of the working face was bigger.
2) Strong ground pressure behavior occurred during the main roof weighting. The strength of weighting is high with long duration time. The safety valve is opened frequently, and the maximum retraction speed of the movable column of the support is 300 mm/h. The depth of the coal wall of the working face can reach more than 1,000 mm.

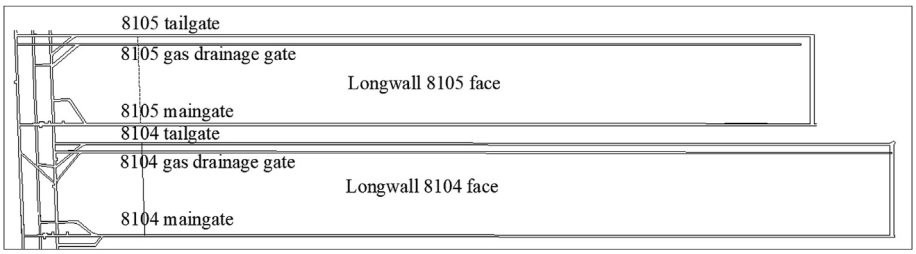

FIGURE 1 | Location map of working faces.

TABLE 1 | Roof and floor strata distribution of 3-5 coal seams.

Number	Strata name	Depth/m	Thickness/m	Uniaxial compressive strength/MPa	Number	Strata name	Depth/m	Thickness/m	Uniaxial compressive strength/MPa
1	Carbonaceous mudstone	460.15	6.30	7.36	23	Siltstone	313.75	3.75	55.73
2	Fine-grained sandstone	453.85	5.85	71.53	24	Mudstone	310	2.40	41.35
3	3–5 coal	448	15.30	15.94	25	Coarse-grained sandstone	307.6	6.75	43.87
4	**Coarse-grained sandstone**	**432.7**	**13.35**	**43.87**	26	Sandy mudstone	300.85	3.00	41.35
5	Siltstone	419.35	7.05	55.73	27	Siltstone	297.85	10.65	55.73
6	Coarse-grained sandstone	412.3	3.15	43.87	28	Medium-grained sandstone	287.2	1.95	56.73
7	Siltstone	409.15	4.35	55.73	29	Fine-grained sandstone	285.25	8.55	71.53
8	Sandy mudstone	404.8	5.55	41.35	30	Siltstone	276.7	17.25	55.73
9	Siltstone	399.25	1.95	55.73	31	Sandy mudstone	259.45	2.25	41.35
10	Fine-grained sandstone	397.3	1.65	71.53	32	Siltstone	257.2	3.15	55.73
11	Siltstone	395.65	2.25	55.73	33	Medium-grained sandstone	254.05	4.65	56.73
12	**Coarse-grained sandstone**	**393.4**	**14.85**	**43.87**	34	Sandy mudstone	249.4	4.80	41.35
13	Siltstone	378.55	4.35	55.73	35	Medium-grained sandstone	244.6	2.25	56.73
14	Coarse-grained sandstone	374.2	3.90	43.87	36	Sandy mudstone	242.35	1.95	41.35
15	Siltstone	370.3	4.95	55.73	37	Medium-grained sandstone	240.4	2.85	56.73
16	Mudstone	365.35	9.60	43.23	38	Sandy mudstone	237.55	17.25	41.35
17	Coarse-grained sandstone	355.75	1.80	43.87	39	Siltstone	220.3	13.95	55.73
18	Mudstone	353.95	3.15	41.35	40	Medium-grained sandstone	206.35	1.95	56.73
19	**Coarse-grained sandstone**	**350.8**	**11.85**	**43.87**	41	Fine-grained sandstone	204.4	5.55	71.53
20	Sandy mudstone	338.95	7.05	41.35	42	Siltstone	198.85	6.30	55.73
21	Coarse-grained sandstone	331.9	2.55	43.87	43	Coarse-grained sandstone	192.55	11.25	43.87
22	Sandy mudstone	329.35	15.60	41.35	44	Siltstone	181.3	19.05	55.73

The bold lines are hard roofs.

3) Under the combined action of the advance pressure of the working face and the roof pressure of the adjacent goaf, the pressure of the gob roadway is relatively large. The roof of the roadway is sinking, the floor is heaving, and the two sides are seriously deformed. The concrete spray layer on the roadway surface cracks and falls (**Figure 2**). The maximum vertical and horizontal convergences were 1.1 and 0.8 m, especially the pillar side is more serious. The steel strip of the roof is deformed in some areas, and the anchor rod is pulled off.

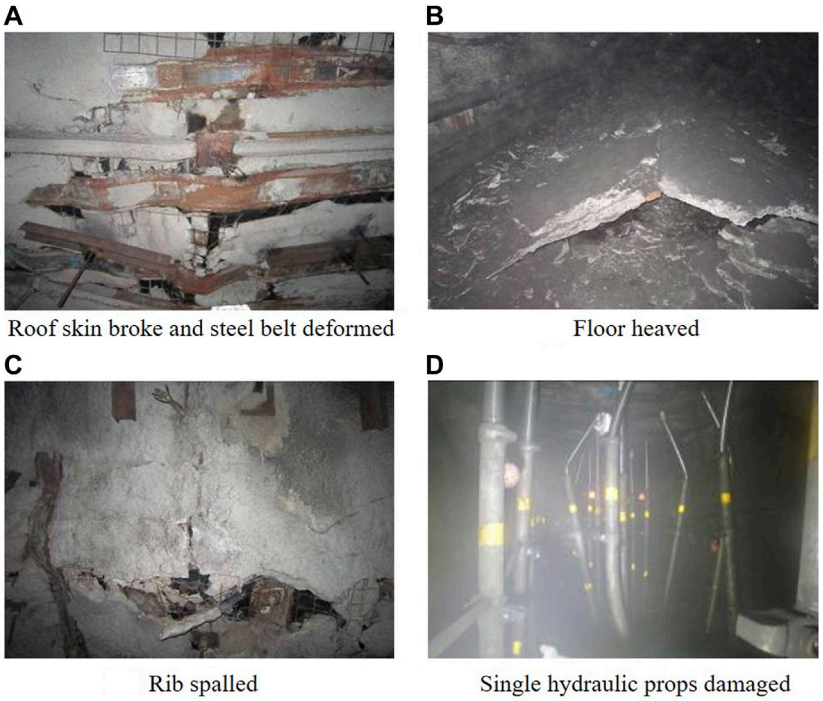

FIGURE 2 | Support damage and roadway floor heave.

TABLE 2 | Mechanical parameters of the strain-softening model.

Shear strain	Cohesion (MPa)	Internal friction angle (°)
0.000	C	Φ
0.005	C	Φ
0.010	C/2	Φ-2.5
0.050	C/5	Φ-5

C is initial cohesion, Φ is initial internal friction angle.

TABLE 3 | Estimated stress and strain of goaf materials according to Salamon's theoretical calculation.

Strain	Stress (MPa)
0	0
0.01	0.66
0.02	1.41
0.03	2.28
0.04	3.3
0.05	4.5
0.06	5.96
0.07	7.74
0.08	9.98
0.09	12.9
0.10	16.8
0.11	22.3
0.12	30.8
0.13	45.3
0.14	76
0.15	185

3 ESTABLISHMENT OF THE NUMERICAL MODEL

3.1 Selection of Constitutive Models

1) Strain-softening model for coal and rock simulation

After the stress peaks, the strength of the rock drops rapidly to a lower level as the deformation continues to increase, a phenomenon known as "strain softening". The strain-softening model believes that the properties of rock materials change with the plasticity. After plastic yielding begins, the cohesion, internal friction angle, and dilatancy angle of the rock will all attenuate with the plastic strain constantly. In the numerical simulation calculation, the strain-softening model can truly reflect the failure of the surrounding rock. Thus, this model is extensively applied in the fields of rock mechanics, geotechnical, and mining engineering. The softening parameters are shown in **Table 2**, and the internal friction angle and the cohesion of the coal and rock change with shear strain.

2) Double-yield model for goaf simulation

The gangue collapsed in the goaf is in a loose state at first and is gradually compacted under the action of its own gravity and overlying rock pressure as the working face advances. The strength and modulus of the rock mass in

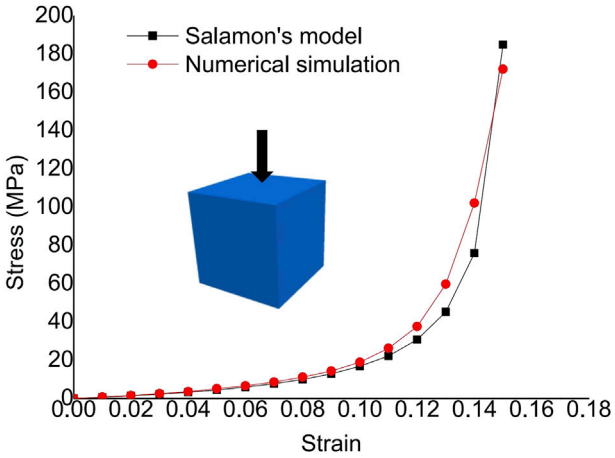

FIGURE 3 | Stress–strain curve comparison between Salamon theoretical analysis and numerical simulation.

the caving zone increase gradually during the gradual compaction process, but it is impossible to reach its original state. This progressively compacted property can be simulated using the double-yield model in FLAC3D. The double-yield constitutive model proposed by Salamon (Salamon 1990) is widely used to analyze the mechanical properties of goaf materials. The formulae are shown below:

$$\sigma = \frac{E_0 \varepsilon}{1 - \varepsilon/\varepsilon_m}, \tag{1}$$

$$\varepsilon_m = \frac{b-1}{b}, \tag{2}$$

$$b = \frac{h_{cav} + h_m}{h_{cav}}, \tag{3}$$

$$E_0 = \frac{10.39\sigma_c^{1.042}}{b^{7.7}}. \tag{4}$$

In the equations, ε_m is the maximum strain, E_0 is the initial modulus, b is the bulking factor, hm is the height of the caving zone, h_{cav} is the mining height, and σ_c is the virgin vertical stress. According to the field data of the working face with a mining height of 15.3 m collected by the EH4 magnetotelluric imaging system, it is estimated that the caving height of the goaf is 80 m (Wu et al. 2019). Therefore, the maximum strain and bulking factor of the collapsed rock are calculated to be 0.15 and 1.16 by **Eqs 2**, **3**, respectively. **Eq. 1** is utilized to quantify the goaf displacement for making a comparison with the simulation results. **Table 3** tabulates the stress and strain of goaf materials calculated by Salamon's equations.

In order to obtain the relevant parameters of the double-yield model of the goaf in the Tongxin coal mine, a single cubic model of 1 × 1 m×1 m is established. The parameters of the model are assigned by trial and error until the stress–strain curves match each other, as shown in **Figure 3**. The two curves are in good agreement, confirming the applicability of the double-yield constitutive model in FLAC3D for goaf simulation. The mechanical parameters of the double-yield model determined that the bulk modulus was 8.6 GPa, shear modulus was 6.3 GPa, density was 2000 kg/m^3, cohesion was 0.1 MPa, internal friction angle was 5°, and dilation angle was 6°.

3.2 Model Setup and Mining Process

By taking the 8,104 and 8,105 working faces in the Tongxin coal mine as the engineering background, numerical simulation software FLAC^{3D} is used to establish a model with a size of 400 × 645 × 324.3 m (length × width × height), and the number of the model

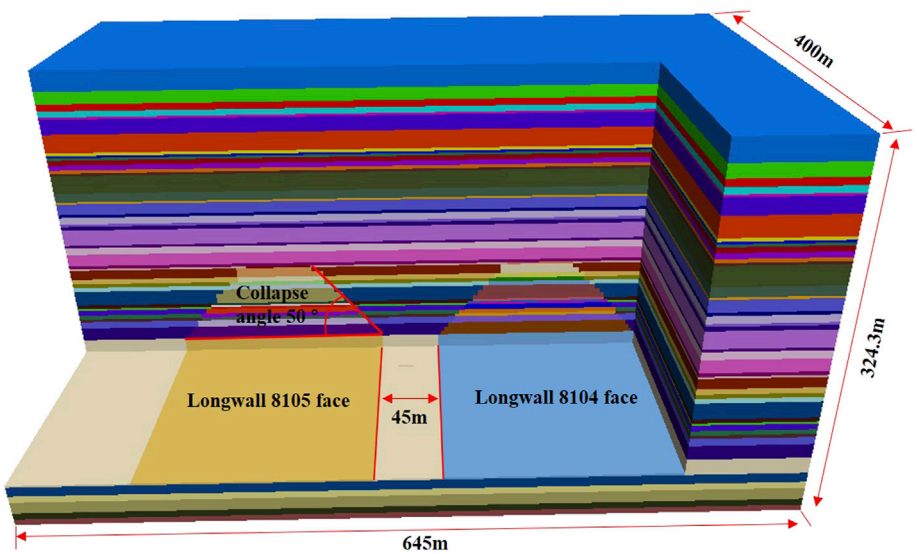

FIGURE 4 | Model stereogram.

TABLE 4 | Mechanical parameters of rock mass in each layer of the model.

Lithology	Density (kg.m-3)	Bulk modulus (GPa)	Shear modulus (GPa)	Internal friction angle (°)	Cohesion (MPa)	Tensile strength (MPa)
Coal	1,373	3.25	1.50	29.9	8.00	1.33
Siltstone	2,532	15.96	10.04	34.6	26.00	4.85
Fine sandstone	2,560	15.98	11.49	34.1	19.80	8.60
Medium sandstone	2,650	17.70	9.80	37.0	17.45	7.10
Grit sandstone	2,383	13.20	10.90	35.7	21.30	6.20
Sandy mudstone	2,570	11.25	7.75	31.3	14.20	4.40
Mudstone	2,747	4.30	2.40	24.0	7.20	2.50
Carbonaceous mudstone	2,728	3.10	1.20	28.0	5.30	2.00

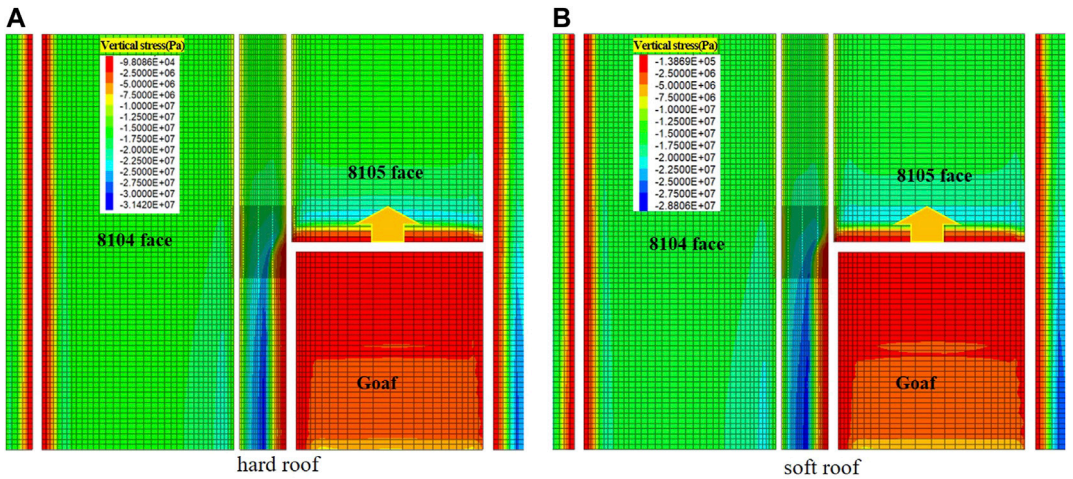

FIGURE 5 | Vertical stress distribution after primary mining under different roof strength conditions.

elements is 758,400 (**Figure 4**). Physical and mechanical parameters are described in **Table 4**. The four sides and the bottom of the model are constrained by displacement. A gradient stress of 15–24.73 MPa is applied in the advancing direction of the working face, and a gradient stress of 12.5–20.6 MPa is applied in the vertical direction of the model.

To accurately investigate the stress distribution in the coal pillar, a 65 × 65 × 65 m grid densification area is established in the middle of the model. Based on the research of Galvin (Galvin 2016), the caving angle of the hard and soft roof is set at 50° and 80°, respectively. In the numerical model of the weak roof, the strength is reduced to 25% of the hard roof. The 8,105 working face is first excavated. After it is completed, mining the 8,104 working face begins. According to the onsite situations in the mine, the 8,104 and 8,105 working faces advance 20 m every step in the numerical model.

4 NUMERICAL SIMULATION RESULTS

4.1 Influence of the Roof Strength on Mining Stress Distribution

1) Mining stress distribution at the working face during the first face advance.

The overhanging state of the roof above the working face varies with different overlying rock strengths. In hard roof conditions, as the working face proceeds, the overhanging area of the roof increases. The working face will bear more abutment pressure, and the roof is not easy to collapse, resulting in strong mining stress. In view of this, the mining stress distribution at the working face is analyzed based on numerical simulation and comparison with the mining process with soft roofs.

Figure 5 shows the mining stress distributions during mining the 8,105 working face in hard and soft roof conditions, respectively. The stress concentration area in front of the working face presents a symmetrical stripe-shape distribution. In hard roof conditions, the influence zone of the front abutment pressure is up to 80 m, the peak stress reaches 26.4 MPa, and the stress concentration factor is 1.84. In soft roof conditions, the influence zone of front abutment pressure is 74 m, the peak stress is 22 MPa, and the stress concentration factor is 1.53.

It can be seen that the roof strength has an obvious influence on the stress concentration area and stress peak value at the mining face. The influence zone of the front abutment pressure is 6 m wider, and the stress peak value is 4.4 MPa higher in hard roof conditions than that in soft roof conditions. The hard

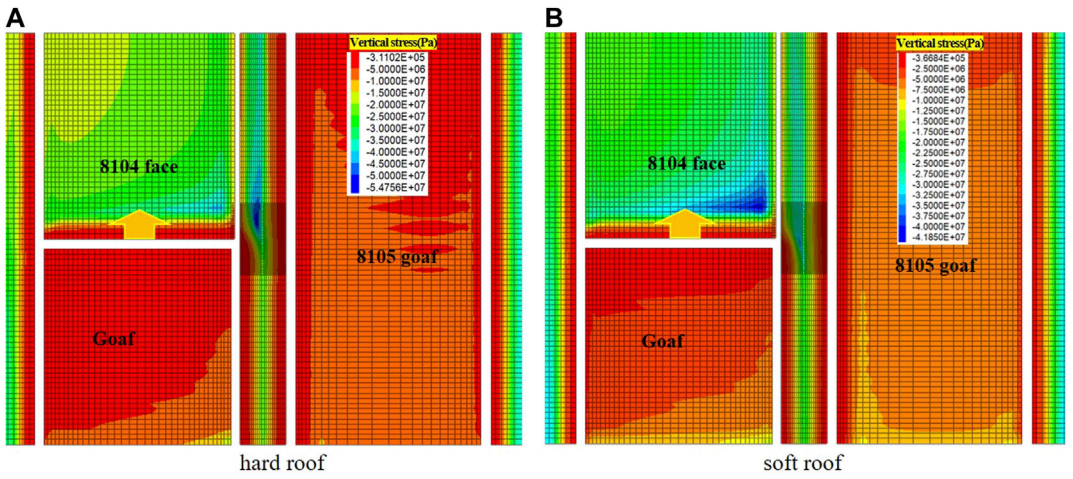

FIGURE 6 | Vertical stress distribution after secondary mining under different roof strength conditions.

overlying strata are more difficult to collapse in the mining process than soft ones and can generate a larger area affected by the higher abutment pressure. Hence, more intense mining stress is produced at the working face during mining the coal seam with a hard roof.

2) Mining stress distribution at the working face during the second face advance.

The stress distributions during mining the 8,104 working face with different roof strengths are compared. In the second mining process, the zone ahead of the working face is affected by two driving disturbances, that is, the influences of the lateral abutment pressure of the adjacent goaf and the front abutment pressure of the working face. The stress will be concentrated in the area close to the goaf, forming a triangular stress concentration zone.

Figure 6 shows the stress distributions in the second excavation under different roof conditions. For hard roof circumstances, the influence range of front abutment stress reaches 97 m, the peak stress increases to 55.4 MPa, and the stress concentration factor gets to 3.85. In the other condition, the influence range of front abutment stress is 91 m, the peak stress is 45 MPa, and the stress concentration factor is 3.13.

It can be seen that the roof strength has a significant impact on the stress concentration zone and stress peak value at the working face. The influence zone of the front abutment pressure is 6 m wider, and the stress peak value is 10.4 MPa higher than a soft overburden. The data indicate that there is greater abutment pressure in front of the working face because the overhanging length of the roof is larger under hard roof conditions. In terms of mining stress, the mining stress at the working face is higher under the condition of a hard overburden, which is more harmful to the safety of the working face.

4.2 Influence of a Hard Roof on Coal Pillar Stability

1) Influence of the roof strength on coal pillar stability in the first face advance

Figure 7 shows the coal pillar after one mining under different roof strengths. It can be seen that the 45-m-wide coal pillar is not completely yielded after the first panel extracted despite different roof conditions. The stability of the coal pillar with different roof strengths has little difference at this time. The width of the plastic zone in the coal pillar under hard roof conditions is the same as that under soft roof conditions. The elastic zone width (14 m) occupies 31.1% of the pillar width (45 m). Due to the influence of the mined-out space, the area of the coal pillar approaching the goaf is destroyed, but the yield zone fails to penetrate through the pillar which is still in a stable state.

The peak stress in the coal pillar with a hard roof is 30.83 MPa which is 4.92 MPa higher than that with a soft roof (25.91 MPa). It is clearly seen from **Figure 8** that the stress exhibits a unimodal-shape distribution due to the effect of the lateral abutment pressure in the goaf. The stress is concentrated in the area close to the solid coal. The lower stress area nearby the goaf indicates that the coal pillar at this region has yielded. The positions bearing the largest stress are basically the same under different roof strengths, but the peak stressed place is much closer to the solid coal under hard roof conditions, and the stress in the coal pillar is also greater.

2) Influence of the roof strength on coal pillar stability in the second face advance

Figure 9 shows the coal pillar after secondary mining under different roof strengths. The plastic zone in the coal pillar is enlarged due to the effects of the two goafs. It can be seen that

Elastoplastic Regional Correlation of the Coal Pillar:

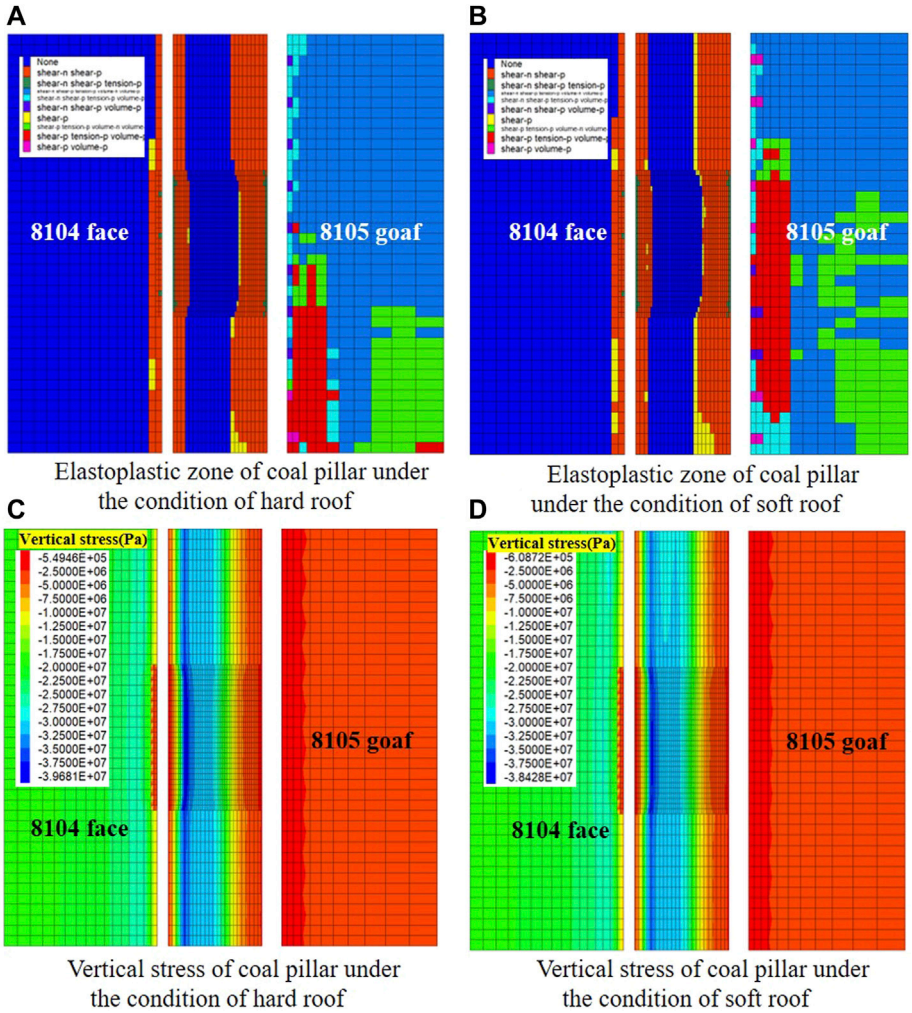

FIGURE 7 | Coal pillar stress and damage after first mining under different roof strength conditions.

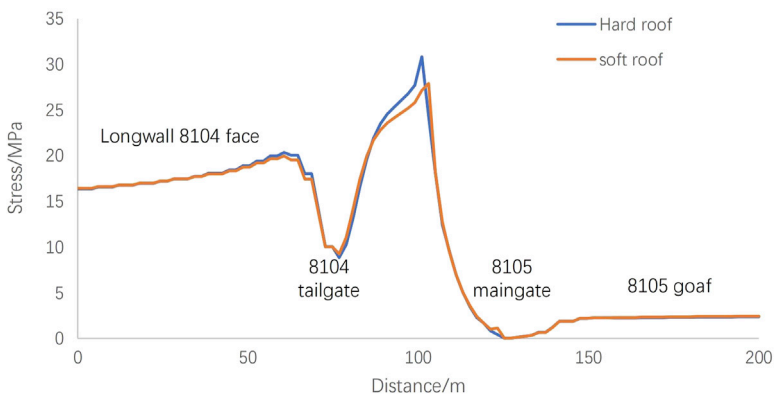

FIGURE 8 | Vertical stress curves in the pillar after the first face was excavated.

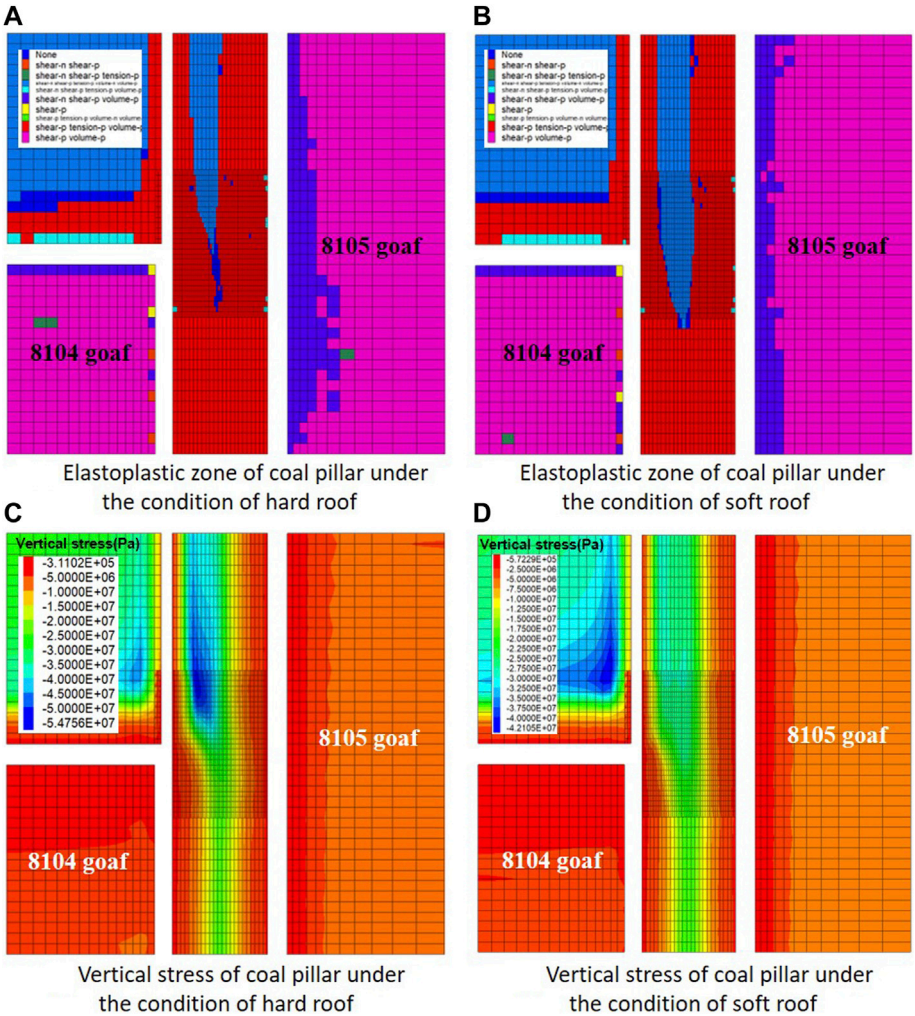

FIGURE 9 | Coal pillar stress and damage after secondary mining under different roof strength conditions.

① At 80 m behind the working face, despite different roof strengths, the 45-m-wide coal pillar is yielded in the whole width, and the coal pillar is completely destabilized owing to the influence of the two goafs.

② At the working face, the elastic zone in the pillar is 5 m, accounting for 11.1% of the total pillar width in hard roof circumstances, while the elastic zone width is 16 m, which is 35.5% of the pillar width in soft roof circumstances. Thereby, hard overlying rocks are unfavorable to the stability of working faces and mining roadways.

③ At 25 m ahead of the working face, the elastic zone width is 11 m, accounting for 24.4% of the pillar width. Regarding the soft roof, the elastic zone is 15 m, that is, 33.3% of the pillar width. The failure zone under hard roof conditions is 4 m wider than that under soft roof conditions. By comparison, the plastic failure zone in the hard roof coal pillar is bigger; the coal pillar is easier to lose stability, the roof is more prone to collapse, and the roadway is easily deformed.

④ At 80 m in front of the working face, for mining with a hard roof structure, the elastic zone width (12 m) is 26.6% of the pillar width. Considering mining the coal seam beneath the soft rock strata, the elastic zone width is 15 m and accounts for 33.3% of the pillar width. The plastic zone width in the first mining situation is 3 m larger than that in the second situation. The comparison shows that the stability of the coal pillar with a hard roof is worse than that with a soft roof, and the roadway is easier to fail.

Comparison of the Stress Distribution Diagram of the Coal Pillar (**Figures 9**, **10**):

① In spite of different roof conditions, the stress has little difference at two monitoring points, namely, 80 m behind the working face and the working face position. The peak stress in the coal pillar under hard roof conditions is 21.9 MPa and that under the other situation is 21.67 MPa. The stress values are quite similar and relatively small, implying that the coal pillar is in a complete yield state.

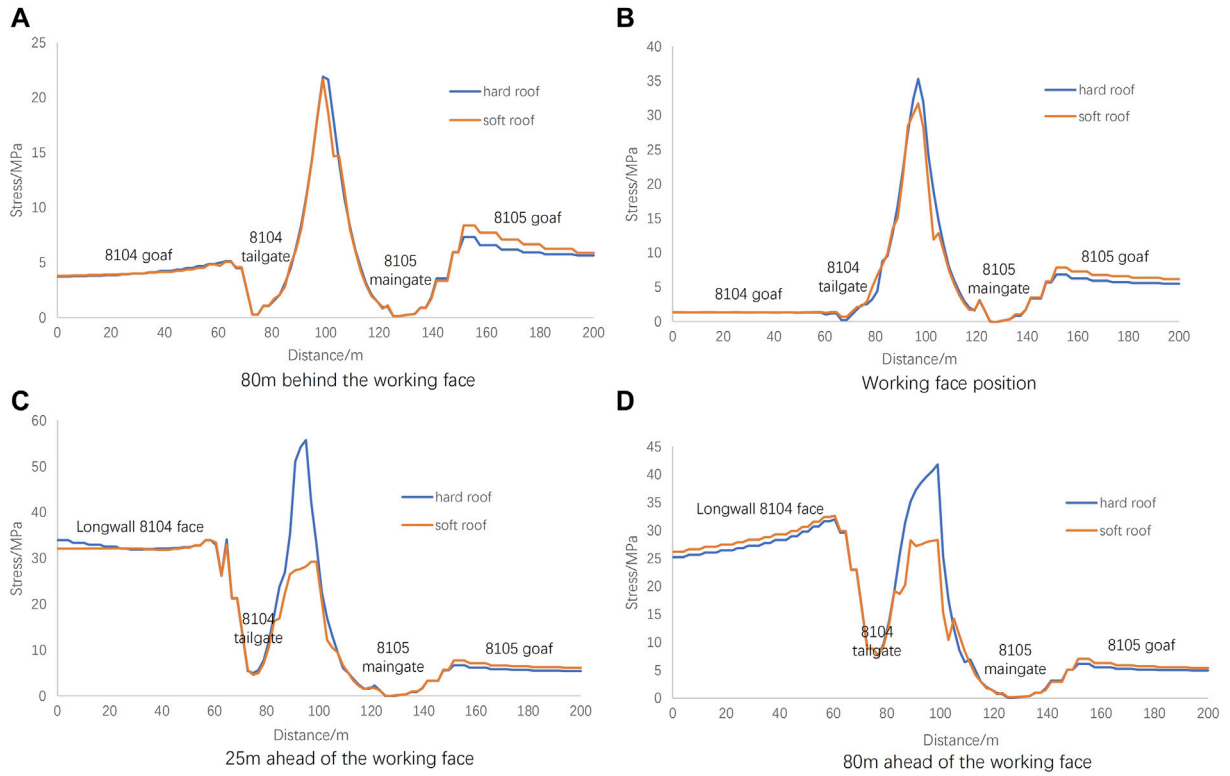

FIGURE 10 | Vertical stress distribution curve of the coal pillar at different positions.

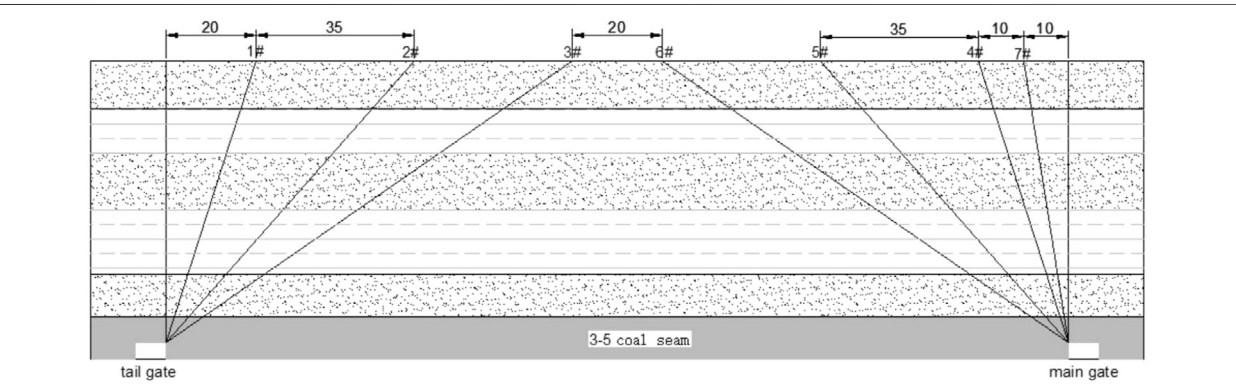

FIGURE 11 | Layout parameters of roof pre-split blasting technology.

② At the face position, the peak stress in the coal pillar with hard overlying strata is 35.27 MPa, which is 5.13 MPa higher than that with soft overlying strata (30.14 MPa). This suggests that the coal pillar is in a relatively low stress state but still in a yield condition, and the coal pillar has a poor load-bearing capacity. The overburden load will impose on the face supports. As a result, the face supports bear more loads, and the working face encounters more mining stress when extracting a coal seam with a hard roof, leading to face support damage and further influencing the stability and safety of the mining roadway and working face.

③ At 25 m in front of the working face, the maximum stress is loaded on the coal pillar. At this position, the difference in peak stress in the coal pillar under different roof strengths is the largest. The peak stress under hard roof conditions (55.76 MPa) is 24.84 MPa higher than that under soft roof circumstances (30.92 MPa). The stress state here manifests that in hard-rock coal mining, the peak stress in front of the working face acts upon the coal pillar, leading to the pillar bearing a greater stress. Hence, the coal pillar is more prone to lose stability, making the working face bear more front abutment pressure.

④ At 80 m ahead of the working face, the peak stress in the coal pillar having a hard roof is 41.77 MPa. It is 13.19 MPa higher than the peak stress in the coal pillar having a soft roof (i.e., 28.58 MPa). This shows that under hard roof conditions, the loads in the coal pillar are larger, and the pillar is easier to fail, and the roadway is more likely to deform.

3) The action mechanism of the hard roof on the working face and pillar system

With the mining of the working face, the roof strata gradually collapsed, and the pressure of the overlying strata was transferred to the coal pillars and the coal body at the goaf boundary. For the mining of extra-thick coal seams, the cantilever beam structure with a height of 80 m is formed because the range of the caving zone is as high as 80 m. For the hard roof, because it is not easy to collapse, the gangue in the goaf cannot support the cantilever beam structure. Moreover, the high-strength roof creates a larger cantilever structure on the horizontal scale. Therefore, most of the overburden pressure acts on the coal walls around the working face and pillars. If the coal pillar does not have sufficient strength, the damage of the cantilever beam structure will occur on the coal body or the coal pillar, further increasing the deformation and damage of the coal pillar. If the coal pillar has high strength, the damage of the cantilever beam structure will occur at the edge of the gob and will not increase the stress of the coal pillar.

5 DISCUSSION

1) Hard roof treatments.

In view of the influence of the hard roof on the working face and coal pillar, the roof pre-split blasting technology can be used to weaken the hard roof. The pre-splitting technology of the hard roof of the working face can destroy the complete overburden structure so that the hard roof can collapse in time and release the stress and energy and reduce damage to the working face due to dynamic load effects. At the same time, in view of the cantilever beam structure formed above the coal pillar, the goaf roof cutting technology is adopted to improve the stress state of the coal pillar and reduce the mine pressure behavior in the adjacent gob roadway. The layout parameters of presplit blasting are shown in **Figure 11**.

2) Limitations of the numerical model.

After the working face is mined, the roof stratum and surrounding rock have plastic failure, and the continuous medium is transformed into a discontinuous medium. The roof of the coal seam forms caving blocks as mining. This article simplifies the roof strata and simulates the gangue in the caving zone with a double-yield constitutive model, which is simplified according to the rock characteristics of the goaf. The surrounding rock of the working face and roadway forms a discontinuous fracture structure. The analysis in this article is based on the continuous medium, and there is a certain error with the actual situation. In the future, the continuous–discontinuous method will be used to study the stability of the coal pillar.

6 CONCLUSION

1) Mining stress evolution rules under different roof strengths are analyzed. It is found that the difference in the mining stress distribution is bigger in the second face mining. The area affected by the front abutment pressure under hard roof conditions is 6 m wider than that under soft roof conditions, and the bearing stress at the working face is 10.4 MPa higher as well.

2) At the mining position, the plastic zone of the pillar under hard roof conditions is 11 m wider than that under soft roof conditions, and the peak vertical stress is 5.13 MPa higher than that under soft roof conditions. At 25 m ahead of the working face, the plastic zone of the pillar under hard roof conditions is 6 m wider than that under soft roof conditions, and the peak vertical stress is 24.84 MPa higher than that under soft roof conditions. The working face beneath the hard overburden is disturbed by greater mining stress, and the roadway is more likely to deform and fail.

3) Concerning strong mine pressure during the working face advance, in view of hard overlying rocks, it is recommended to adopt pre-cracking techniques to reduce the influence of the roof on the appearance of strong mine pressure.

DATA AVAILABILITY STATEMENT

The original contributions presented in the study are included in the article/supplementary material, further inquiries can be directed to the corresponding author.

AUTHOR CONTRIBUTIONS

ZZ contributed to the conception of the study. YW contributed significantly to analysis and manuscript preparation. ZL contributed model analysis.

FUNDING

This work was supported by the State Key Laboratory of Coal Mining and Clean Utilization (2021-CMCU-KF016) and the Basic Scientific Research Projects of Universities in Liaoning Province (LJKZ0343).

ACKNOWLEDGMENTS

The assistance and guidance of the steering group members are gratefully acknowledged.

REFERENCES

Ardehjani, E. A., Ataei, M., and Rafiee, R. (2020). 'Estimation of First and Periodic Roof Weighting Effect Interval in Mechanized Longwall Mining Using Numerical Modeling. *Int. J. Geomechanics* 20, 1–13. doi:10.1061/(asce)gm.1943-5622.0001532

Bai, Q.-S., and Tu, S.-H. (2016). Failure Analysis of a Large Span Longwall Drift under Water-Rich Roofs and its Control Techniques. *Eng. Fail. Anal.* 67, 15–32. doi:10.1016/j.engfailanal.2016.05.028

Das, S. K. (2000). Observations and Classification of Roof Strata Behaviour over Longwall Coal Mining Panels in India. *Int. J. Rock Mech. Mining Sci.* 37, 585–597. doi:10.1016/s1365-1609(99)00123-9

Galvin, J. M. (2016). *Ground Engineering-Principles and Practices for Underground Coal Mining*. Springer.

Hosseini, N., Goshtasbi, K., Oraee-Mirzamani, B., and Gholinejad, M. (2014). Calculation of Periodic Roof Weighting Interval in Longwall Mining Using Finite Element Method. *Arab J. Geosci.* 7, 1951–1956. doi:10.1007/s12517-013-0859-8

Ju, M., Wang, D., Shi, J., Li, J., Yao, Q., and Xing, L. (2021). 'Physical and Numerical Investigations of Bedding Adhesion Strength on Stratified Rock Roof Fracture with Longwall Coal Mining. *Geomechanics Geophys. Geo-Energy Geo-Resources* 7, 1–31. doi:10.1007/s40948-020-00209-2

Juárez-Ferreras, R., González-Nicieza, C., Menéndez-Díaz, A., Álvarez-Vigil, A. E., and Álvarez-Fernández, M. I. (2008). Measurement and Analysis of the Roof Pressure on Hydraulic Props in Longwall. *Int. J. Coal Geology.* 75, 49–62. doi:10.1016/j.coal.2008.01.007

Kang, H., Lou, J., Gao, F., Yang, J., and Li, J. (2018). A Physical and Numerical Investigation of Sudden Massive Roof Collapse during Longwall Coal Retreat Mining. *Int. J. Coal Geology.* 188, 25–36. doi:10.1016/j.coal.2018.01.013

Liu, C., Li, H., Mitri, H., Jiang, D., Li, H., and Feng, J. (2017). Voussoir Beam Model for Lower strong Roof Strata Movement in Longwall Mining - Case Study. *J. Rock Mech. Geotechnical Eng.* 9, 1171–1176. doi:10.1016/j.jrmge.2017.07.002

Liu, J., Li, C., Shi, Y., and Zhang, Y. (2021). Stability Analysis and Fracture Patterns of Hard Main Roof in Longwall Top Coal Caving with Large Mining Height. *Shock and Vibration* 2021, 9930221. doi:10.1155/2021/9930221

Mahini, M. R., Moharrami, H., and Cocchetti, G. (2013). A Dissipated Energy Maximization Approach to Elastic-Perfectly Plastic Analysis of Planar Frames. *Arch. Mech.* 65, 171–194.

Mohammadi, S., Ataei, M., Kakaie, R., Mirzaghorbanali, A., and Aziz, N. (2021). A Probabilistic Model to Determine Main Caving Span by Evaluating Cavability of Immediate Roof Strata in Longwall Mining. *Geotech Geol. Eng.* 39, 2221–2237. doi:10.1007/s10706-020-01620-y

Murmu, S., and Budi, G. (2021). A Probability-Based Risk Assessment of Roof Strata Weighting in Longwall Panels. *Arabian J. Geosciences* 14, 1–16. doi:10.1007/s12517-021-06637-y

Ning, J., Wang, J., Jiang, L., Jiang, N., Liu, X., and Jiang, J. (2017). Fracture Analysis of Double-Layer Hard and Thick Roof and the Controlling Effect on Strata Behavior: A Case Study. *Eng. Fail. Anal.* 81, 117–134. doi:10.1016/j.engfailanal.2017.07.029

Qin, S., Li, Y., and Sun, L. (2019). 'Stability Evaluation of Karst Cave Roof under Pile in Karst Areas Based on the Interval Non-probabilistic Reliability Method. *Hydrogeology Eng. Geology.* 46, 81–88. doi:10.16030/j.cnki.issn.1000-3665.2019.05.11

Rajwa, S., Janoszek, T., and Prusek, S. (2020). 'Model Tests of the Effect of Active Roof Support on the Working Stability of a Longwall. *Comput. Geotechnics* 118, 103302. doi:10.1016/j.compgeo.2019.103302

Salamon, M. D. G. (1990). "Mechanism of Caving in Longwall Coal Mining," in *Rock Mechanics Contributions and Challenges: Proceedings of the 31st US Symposium* (Golden, Colorado: Publ Rotterdam, 161–168.

Wang, H., Chen, X., Zhou, Y., Xia, B., Wang, J., Zhao, S., et al. (2020). A Method Based on Elastic Mechanics for Judging Compound Hard Roof and its Application. *Shock and Vibration* 2020, 8867259. doi:10.1155/2020/8867259

Wu, W.-D., Bai, J.-B., Wang, X.-Y., Zhu, Z.-J., and Yan, S. (2019). Field Investigation of Fractures Evolution in Overlying Strata Caused by Extraction of the Jurassic and Carboniferous Coal Seams and its Application: Case Study. *International Journal of Coal Geology* 208, 12–23. doi:10.1016/j.coal.2019.04.002

Xu, T., Yang, T.-h., Chen, C.-f., Liu, H.-l., and Yu, Q.-l. (2015). Mining Induced Strata Movement and Roof Behavior in Underground Coal Mine. *Geomech. Geophys. Geo-energ. Geo-resour.* 1, 79–89. doi:10.1007/s40948-015-0010-2

Yang, S., Wang, J., Li, X., Ning, J., and Qiu, P. (2019). *In Situ* investigations into Mining-Induced Hard Main Roof Fracture in Longwall Mining: A Case Study. *Eng. Fail. Anal.* 106, 104188. doi:10.1016/j.engfailanal.2019.104188

Yang, Z. L. (2010). Stability of Nearly Horizontal Roof Strata in Shallow Seam Longwall Mining. *Int. J. Rock Mech. Mining Sci.* 47, 672–677. doi:10.1016/j.ijrmms.2010.03.001

Zhang, H., Cao, Y., Zhu, F., and Shao, L. (2018). 'Precursor Discrimination and Mechanism of Rock Burst in the Island Workface with Hard Roof. *Coal Geology. Exploration* 46, 118–123. doi:10.3969/j.issn.1001-1986.2018.02.018

Zhang, J., Zhang, Y., Du, W., Wang, H., and Serati, M. (2021). An Analytical Approach to Estimate the Mechanical State of Roof Strata in Underground Longwall Mining. *Geomechanics Eng.* 27, 55–62. doi:10.12989/gae.2021.27.1.055

Zonglong, M. U., Linming, D. O. U., Zhang, G., Zhang, S., Zhihua, L. I., and Zhang, J. (2006). Study of Prevention Methods of Rock Burst Disaster Caused by Hard Rock Roof. *J. China Univ. Mining Technology. Nat. Sci.* 35, 737–741. doi:10.1093/carcin/bgm010

Conflict of Interest: The authors declare that the research was conducted in the absence of any commercial or financial relationships that could be construed as a potential conflict of interest.

Publisher's Note: All claims expressed in this article are solely those of the authors and do not necessarily represent those of their affiliated organizations, or those of the publisher, the editors, and the reviewers. Any product that may be evaluated in this article, or claim that may be made by its manufacturer, is not guaranteed or endorsed by the publisher.

Copyright © 2022 Zhu, Wu and Liang. This is an open-access article distributed under the terms of the Creative Commons Attribution License (CC BY). The use, distribution or reproduction in other forums is permitted, provided the original author(s) and the copyright owner(s) are credited and that the original publication in this journal is cited, in accordance with accepted academic practice. No use, distribution or reproduction is permitted which does not comply with these terms.